Received: 17 July 2023 | Accepted: 17 November 2023

DOI: 10.1002/vzj2.20301

Vadose Zone Journal

ORIGINAL ARTICLE

Biochar modifies soil physical properties mostly through changes in soil structure rather than through its internal porosity

Martin Zanutel[1] | **Sarah Garré**[2] | **Patrick Sanglier**[3] | **Charles Bielders**[1]

[1]Earth and Life Institute, UCLouvain, Louvain-la-Neuve, Belgium

[2]Flanders Research Center for Agriculture, Fisheries and Food (ILVO), Merelbeke, Belgium

[3]Laboratory of Inorganic Materials Chemistry, UNamur, Namur, Belgium

Correspondence
Martin Zanutel, Earth and Life Institute, UCLouvain, Croix du sud 2, bte L7.05.02, B-1348, Louvain-la-Neuve, Belgium.
Email: martin.zanutel@uclouvain.be

Assigned to Associate Editor Emmanuel Arthur.

Funding information
Fonds De La Recherche Scientifique—FNRS, Grant/Award Number: FC036167

Abstract

Besides its carbon sequestration potential, biochar application generally improves soil physical properties, but the magnitude of its impact and the underlying mechanisms remain debated and depend on soil type, biochar application rate, and age. The objective was therefore to determine the effect of biochar application rate and age on physical properties of agricultural soils in a temperate climate. On a silt loam and a sandy loam soils, we compared the physical properties of fresh biochar (1% and 2% w/w) or century-old biochar (0.5%–1% w/w; 19th-century kiln sites)-enriched soil samples with biochar-free soil samples. Biochar pore network characteristics were determined using helium pycnometry, mercury intrusion porosimetry, scanning electron microscopy observation, and electron dispersive X-ray spectrometry, whereas location of biochar particles within soil structure was analyzed using optical microscopy observations. Fresh biochar application decreased bulk density by 16.8% and increased saturated water content by 16.0% and macroporosity by 78.8%. These effects were attributed to soil structure improvement rather than to biochar porosity. Soil type and biochar application rate had a limited impact. In the long-term, biochar effects were mostly nonsignificant, which might result from its fairly low content in kiln sites and from the clogging of its internal porosity by clay particles. Biochar was thus able to improve some soil physical properties in the short-term, but these effects could no longer be detected in the very long-term. Further investigating the time rate of change in soil physical properties over several decades following biochar additions to soil would therefore seem particularly relevant.

1 | INTRODUCTION

Soil structure is a crucial component of soil quality (Pagliai et al., 2004), and soil organic matter (SOM) plays a key role in the development of soil structure (Abiven et al., 2009; Boyle et al., 1989; Kong et al., 2005). Given the widespread decline in SOM in cultivated soils (EC, 2006; Goidts & van Wesemael, 2007; Poeplau & Dechow, 2023; Prietzel et al., 2016; Whitehead et al., 2021), numerous strategies to increase SOM content in the topsoil have been tested and documented (e.g., organic amendments, cover crops, conservation tillage, and adapted crop rotations; Berhane et al., 2020; De Stephano & Jacobson, 2017; Luo et al., 2010; Payen et al., 2021; Poeplau & Don, 2015). Nevertheless, raising SOM content is

Abbreviations: EDS, energy dispersive X-ray spectrometry; MIP, mercury intrusion porosimetry; PCA, principal component analysis; SEM, scanning electron microscopy.

usually a slow process and can be hampered by regulations surrounding nitrogen management. Recently, there has been a growing interest in biochar for use as a soil amendment to enhance soil aggregation and structure (Juriga & Šimanský, 2018; Lee et al., 2021). Biochar is derived from the pyrolysis of renewable carbon sources such as crop residues and wood (Lehmann et al., 2021). Because biochar has a high carbon content and is not easily degraded, burying biochar in soils also sequesters carbon (Purakayastha et al., 2015; Woolf et al., 2010). Furthermore, biochar is able to retain cations due to its surface charges (Mia et al., 2017; Shaaban et al., 2013). Hence, biochar has multiple benefits, which may make it more amenable to adoption than other types of soil conditioners.

Zanutel et al. (2021) summarized four ways by which biochar can affect soil structure and the soil porosity pattern. Following the addition of biochar to soil, soil porosity may be modified (1) through the intrinsic porosity of biochar particles (Brewer et al., 2014; Hyväluoma et al., 2018; Lehmann & Joseph, 2009; Yi et al., 2020) or (2) through its location and interaction with soil structure by (2a) filling voids in between mineral grains, especially in coarse-textured soils (Edeh et al., 2020), (2b) occupying space previously occupied by mineral particles or organo-mineral micromass, or (2c) acting as an additional binding agent resulting in a soil structuring effect similar to the addition of uncharred organic matter (Burgeon et al., 2021; Du et al., 2017). Through indirect effects on soil biology (Li et al., 2020; Wang et al., 2023; Zhang et al., 2018) and uncharred organic matter content (Burgeon et al., 2021; Hardy et al., 2016; Hernandez-Soriano et al., 2015; Kerré et al., 2016), biochar addition to soil may also result in a structuring effect, although this effect cannot be isolated from the direct effects of biochar addition to soils.

Several authors have summarized the literature linking biochar amendments to soil structure. Quantifying changes in soil structure is most often done through conventional measurements of soil physical properties (e.g., bulk density and porosity, water retention curve, hydraulic conductivity curve), which are strongly linked to soil structure (Pagliai et al., 2004). The reviews of Blanco-Canqui (2017, 2021) and the meta-analysis of Razzaghi et al. (2020) reported that the application of biochar on average decreases bulk density and increases porosity as well as plant available water content, especially in coarse-textured soils. However, Borchard et al. (2014), Jeffery et al. (2015), and Zhang et al. (2015) observed a negative or negligible impact of biochar on these properties, indicating that the effect of biochar may be context dependent. Regarding the saturated hydraulic conductivity, while the meta-analysis of Omondi et al. (2016) reported higher saturated hydraulic conductivity in biochar-enriched soil irrespective of soil texture, the review of Blanco-Canqui (2017) and the meta-analysis of Edeh et al. (2020) revealed that this property tends to decrease in coarse-textured soils, is not significantly affected in medium-textured soils and tends to increase in fine-textured soils upon application of biochar. Therefore, the overall effects of biochar amendments on soil structure can be positive, negligible, or negative. The sign and extent of the effect appear to depend on initial soil properties but biochar properties and biochar application rates must also be taken into account (Gholamahmadi et al., 2023; Islam et al., 2021; Omondi et al., 2016; Singh et al., 2022). The meta-analysis of Razzaghi et al. (2020) thus highlighted the need to carry out additional experiments to allow better elucidation of the mechanisms underlying biochar's impact.

Numerous studies have assessed the impact of biochar additions to soils on the above-mentioned properties in short-term experiments (<5 years after application). However, biochar will remain in soils for hundreds or even thousands of years due to its strong resistance to degradation (Gurwick et al., 2013). During this time, its properties gradually change due to particle fragmentation and the oxidation of its surface (a process referred to as "biochar aging"), leading to an increase in its surface charges and greater interactions with the soil organo-mineral components (Hardy et al., 2016, 2017). Therefore, one may expect the long-term effects of biochar on soil structure to be enhanced compared to the short-term effects. For lack of long-term experiments, the long-term effects of biochar can be investigated by using kiln sites as proxy. Kiln sites refer to areas where charcoal was produced in kilns in situ to be used as fuel for the metallurgical industries until the end of the first half of the 19th century (Hardy & Dufey, 2015). Nowadays, leftover charcoal is found in soil at these former kiln sites, which have consequently been used as a natural model to study the long-term impact of wood-derived biochar (Burgeon et al., 2021, 2022; Hardy et al., 2016, 2019; Hernandez-Soriano et al., 2015; Kerré et al., 2016, Kerré, Willaert, Cornelis et al., 2017, Kerré, Willaert, Smolders et al., 2017; Pollet et al., 2022; Zanutel et al., 2021). Using kiln sites as a proxy, Kerré, Willaert, Cornelis et al. (2017) observed higher saturated water

Core Ideas

- The effect of biochar age and concentration on soil physical properties was studied.
- Young biochar reduced bulk density and increased saturated water content and macroporosity.
- Biochar effects were attributed to soil structure improvement rather than to its internal pore characteristics.
- Century-old biochar in kiln sites did not significantly affect soil physical properties.
- Soil type and biochar application rate impacted the results to a limited extent.

TABLE 1 Characteristics of the study sites and related soils.

Variables	Units	La Bruyère	Attert
Latitude	N (°)	4.76	5.82
Longitude	E (°)	50.53	49.74
Average (1991–2020) annual temperature	°C	10.2	9.1
Average (1991–2020) annual precipitation	mm	805	1136
Mean slope	%	3	4
Textural class (USDA classification)	–	Silt loam	Sandy loam
Sand content	%	2.9 ± 0.1	60.6 ± 4.9
Silt content	%	84.3 ± 0.4	24.3 ± 4.6
Clay content	%	12.8 ± 0.3	15.1 ± 1.6
Gravel content	%	0.9 ± 0.1	2.3 ± 0.4
Soil organic carbon content (REF)	g kg^{-1}	11.6 ± 0.3	19.6 ± 2.3
Biochar content in kiln sites (OB)	g kg^{-1}	7.4 ± 0.3	6.2 ± 1.7
pH-KCl (REF)	–	6.9 ± 0.1	5.8 ± 0.1
Cation exchange capacity (REF)	$cmol_c$ kg^{-1}	8.6 ± 0.1	6.2 ± 0.6
Exchangeable Ca^{2+} content (REF)	$cmol_c$ kg^{-1}	10.17 ± 0.49	6.98 ± 0.57
Exchangeable Mg^{2+} content (REF)	$cmol_c$ kg^{-1}	0.53 ± 0.04	1.54 ± 0.15
Exchangeable K^{+} content (REF)	$cmol_c$ kg^{-1}	0.41 ± 0.01	0.89 ± 0.18

Note: REF and OB correspond to the reference and old biochar subplots, respectively. Data are means ± standard errors of the means.

content and plant-available water content for soils containing century-old biochar (OB) compared to adjacent soils. On the contrary, Zanutel et al. (2021) reported a limited effect of centennial biochar on soil physical properties. Overall, the long-term impact of biochar on soil physical properties remains poorly studied, unclear, and requires more investigation, as also indicated by the meta-analysis of Singh et al. (2022).

Due to its porous structure and its ability to affect soil structure, we hypothesized that the presence of biochar in soil can improve soil physical properties in both the short-term and long-term. The effect of biochar was expected to increase with increasing biochar application rates. At equivalent biochar contents, its effect was expected to be stronger in the long term than in the short term because of biochar fragmentation and aging. The present study therefore aimed at determining the effect of biochar application on soil physical properties on cropland in temperate climate and to assess whether this effect depends on biochar application rate and age.

2 | MATERIALS AND METHODS

2.1 | Study sites and sampling

Two conventionally cropped fields were selected as study sites in the municipalities of La Bruyère (loam region) and Attert (Belgian Lorraine) in Wallonia (southern Belgium, Figure 1), which is characterized by an oceanic temperate climate (Table 1). The study fields were selected because they differ in terms of soil texture and because of the presence of former kiln sites a few decameters in diameter. The soils of the study fields are characterized by a silt loam texture in La Bruyère and a sandy loam texture in Attert (Table 1). Additional characteristics of the study sites are provided in Table 1. In La Bruyère, a 4-year crop rotation involving chicory, winter wheat, sugar beet, potatoes, and cover crops (mustard and phacelia) has been practiced for more than 30 years. In Attert, maize has been cultivated continuously for more than 50 years, with cover crops during winter.

At both study sites, four treatments (6-m by 3-m subplots) were established in triplicate (Figure 1). The first two treatments corresponded to fresh biochar added at an application rate of 13.5 Mg ha^{-1} (YB1%) and 27 Mg ha^{-1} (YB2%) to study the short-term impact of biochar. These application rates were chosen to achieve a biochar content of 1% and 2% by weight, respectively, considering incorporation in the top 10 cm of the soil and a mean soil bulk density of 1350 kg m^{-3}. The third treatment corresponded to the center of kiln sites (OB), containing charcoal dating back most likely from the first half of the 19th century, to study the effect of century-old biochar. The last treatment corresponded to the control (REF), that is, locations without biochar chosen in the same fields. All REF, YB1%, and YB2% subplots were located more than 20 m away from each kiln site to limit the presence of century-old biochar residues in soils (Figure 1).

The fresh biochar was bought from a local biochar producer (GreenPoch SA). European Biochar Certificate

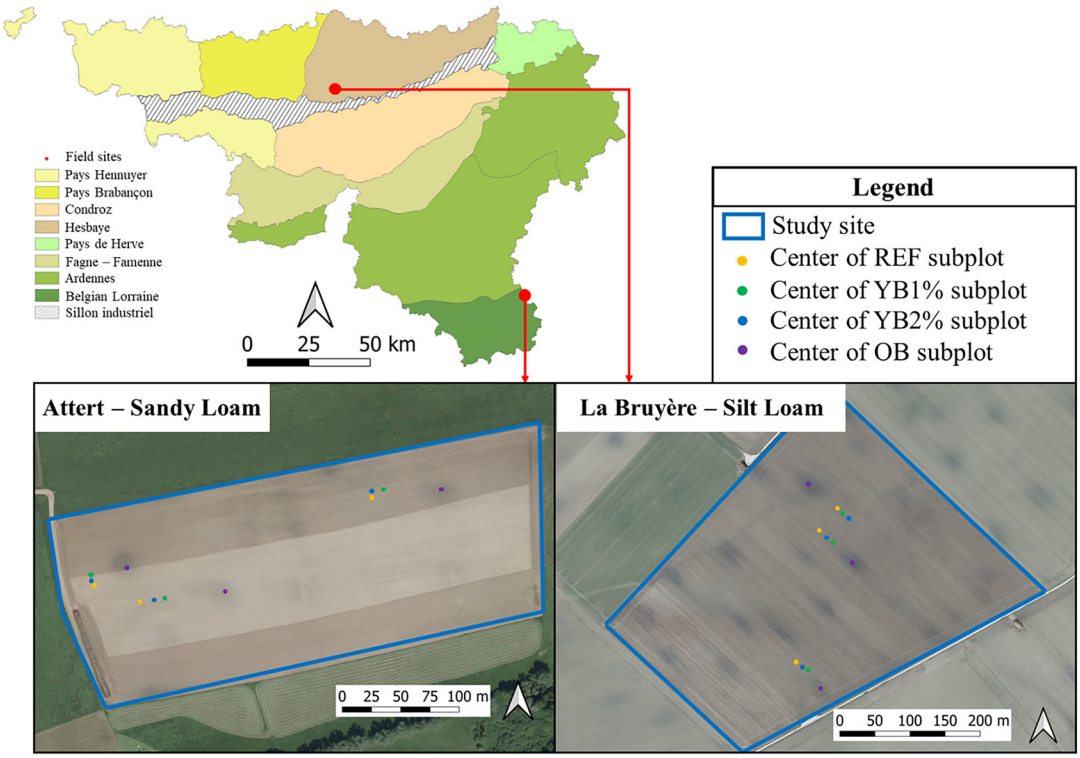

FIGURE 1 Location of study sites on the Belgian map of agro-geographic areas and aerial views of fields in La Bruyère (2021; silt loam soil) and Attert (2012; sandy loam soil) with location of the subplots. REF, YB1% and YB2%, and OB subplots correspond, respectively, to the reference subplots, young biochar subplots enriched at rates of 1% and 2% by weight, and old biochar subplots in kiln sites. Kiln sites are visible as darker oval spots.

certified biochar with a carbon content of 81% by weight and a pH of 8.9 was used. It had been produced from *Picea abies* wood with an industrial pyrolizer at 500˚C. The water drop penetration time test (Doerr, 1998) revealed that biochar particles were hydrophilic (penetration time <1 s for 64 µL water drops). 61.5% by weight of the biochar particles were bigger than 2 mm. The mean weight diameter was 3.1 mm. Biochar particles were applied manually in 2021 at the soil surface before being incorporated into the soil to a depth of 10 cm by tillage (rototiller) immediately prior to sowing of the spring crop. The spring crops were sown on April 21 in La Bruyère (sugar beet) and on May 9, 2021 in Attert (maize).

The topsoil (0–10 cm) was sampled twice at both study sites, approximately 4 and 5 months after sowing of the spring crops. The samplings occurred on August 18–19 and September 22–23, 2021 in La Bruyère, and on September 1 and October 7, 2021 in Attert. For each sampling date and subplot, bulk soil samples were taken for soil characterization. Three undisturbed soil samples (250-cm^3 ring) were also taken on each date and subplot for determination of physical properties. Moreover, undisturbed soil blocks in boxes (8.5 cm × 5.5 cm × 4 cm; Polyvinyl chloride) were sampled on the second sampling date for optical microscopy observations on soil thin sections. Bulk soil samples were air-dried, whereas undisturbed soil samples were stored at 4˚C. Data from both sampling dates were treated as replicates.

2.2 | Soil physical properties

Both the water retention curve and the hydraulic conductivity curve were determined on one of the three 250-cm^3 undisturbed soil cores per subplot and per sampling date, leading to a total of six water retention and hydraulic conductivity curves for each treatment at both study sites. The soil cores were first saturated by capillarity standing in a 0.05 M $CaSO_4$ solution for at least 72 h. The volumetric saturated water content of the soil cores was determined by dividing the difference between the masses of water-saturated and oven-dried soil by the volume of the soil cores. Both the water retention curves and the hydraulic conductivity curves were measured using a HYPROP device (METER Group). The method relies on the monitoring of water content, pressure head, and hydraulic head gradient in an initially saturated sample subjected to evaporation (Pertassek et al., 2015). The pressure head (tensiometers) at two depths in the soil core as well as the water content (sample weight) were measured

every 10 min during drying by evaporation. Soil hydraulic conductivity was derived from water flux measurements (rate of water loss by evaporation) and the total hydraulic head gradient using Darcy's law as described in Pertassek et al. (2015). With the HYPROP device, hydraulic conductivity measurements are constrained by (too) small pressure head differences on the wet end of the hydraulic conductivity curve and by cavitation of the tensiometers on the dry end (Pertassek et al., 2015). Cavitation in the tensiometers occurred between pF 2.8 and 3.5 (Schindler et al., 2010). Regarding the water retention curves, additional data were collected using a pressure plate apparatus (pF = 3.5 and pF = 4.2; Richards & Fireman, 1943) and a WP4C device (pF > 4; METER Group, 2018). Water retention and hydraulic conductivity curve models were fitted to the experimental data (Peters & Durner, 2008). In the present study, the same model was used to fit the data from all samples to be able to compare the results across sites and treatments. The bimodal Durner model was used because of the bimodal pore size distribution observed in most datasets (Durner, 1994).

The macro-, meso-, and microporosity were determined based on the fitted water retention curves. Given the lack of standardization, field capacity (pF = 2) and permanent wilting point (pF = 4.2) were chosen to define the limits between macro- and mesopores and between meso- and micropores, respectively. Moreover, the soil pore size distribution was derived from the water retention curve model using Jurin's law (Equation 1), assuming a solid–liquid contact angle of 0° (Li & Zhang, 2009; Muñoz-Castelblanco et al., 2012; Or & Wraith, 2002; Schäffer et al., 2013):

$$|h| = \frac{4\,\tau\cos(\beta)}{\rho\,g\,d} \tag{1}$$

where h is the matric head (m), τ is the surface tension of water (kg s^{-2}), β is the solid–liquid contact angle (°), ρ is the water density (kg m^{-3}), g is the acceleration due to gravity (m s^{-2}), and d is the pore diameter (m).

Soil bulk density was determined by dividing the oven-dry soil mass (105°C, 48 h) of the soil cores by the volume of the soil sample (250 cm^3). All undisturbed soil cores were used for this purpose. To assess the impact of the intrinsic porosity of biochar particles on soil bulk density, the mass and volume of biochar in biochar-enriched samples were subtracted from the original dry soil mass and volume to calculate the soil bulk density without the direct contribution of biochar, as proposed by Hardie et al. (2014) and also used by Andrenelli et al. (2016).

Finally, a single-ring infiltrometer was used to determine the saturated hydraulic conductivity directly in situ. On each subplot of both study sites for each sampling date, three replicate measurements were conducted, leading to a total of 144 measurements. The saturated hydraulic conductivity was derived from the water flux measurements using Equation (2) (Reynolds & Elrick, 1990) as follows:

$$Ks = \frac{GQ}{aH + \pi a^2 G + a/\alpha} \tag{2}$$

where K_s is the saturated hydraulic conductivity (m s^{-1}), G is a shape parameter defined according to the geometry of the system (-), Q is the water flow (m^3 s^{-1}), a is the radius of the infiltration ring (m), H is the depth of ponding (m), and α is the shape parameter from the equation of Gardner (1958) (m^{-1}). The G and α parameters were set to 0.383 (0.432) and 12 (36) m^{-1} for the silt loam (the sandy loam) soil based on the tables provided by Reynolds and Elrick (1990).

2.3 | Biochar pore network characterization

A few grams of century-old biochar particles were manually isolated from both soils by wet sieving (1-mm mesh), using a methodology similar to Hardy et al. (2017). The old biochar particles could be distinguished from other soil components based on their low density (light weight) and black color. The characteristics of the fresh and old biochar pore network were determined using helium pycnometry, mercury intrusion porosimetry (MIP), and scanning electron microscopy (SEM). Electron dispersive X-ray spectrometry (EDS) was used to characterize the surface composition of biochar.

2.4 | Helium pycnometry and mercury intrusion porosimetry

The following measurements were performed on fresh and old biochar particles in triplicate. Particle density was determined on 1–1.5 g of biochar by means of helium pycnometry using an Anton Paar Ultrapyc 5000 automatic gas pycnometer (Anton Paar, 2023). Particle density of each sample was derived from the mean of 12 successive measurements on the same sample. Bulk density and pore size distribution of biochar particles were determined by means of MIP using a Micromeritics Autopore IV 9500 mercury porosimeter (Micromeritics, 2017), assuming a cylindrical pore model, a mercury (Hg)–soil contact angle of 130°, and a Hg surface tension of 0.485 N m^{-1} (Klock et al., 1969; Lawrence, 1977). The porosimeter can accommodate a sample with a bulk volume of maximum 15 cm^3. In practice, the masses of biochar used in the porosimeter ranged from 0.2 to 0.5 g for young biochar and from 1 to 3 g for old biochar. The difference in mass between old and young biochar stems from the large differences in biochar bulk densities (see results section). Biochar bulk density refers to the mass of the biochar particles divided by the total volume of the particles, including internal voids. Porosity of biochar particles was calculated

according to Equation (3). The porosity calculated with this method does not consider the occluded porosity and therefore corresponds to the porosity accessible to external liquid.

$$\text{Porosity} = 1 - \frac{\text{Bulk density}}{\text{Particle density}} \quad (3)$$

2.5 | Scanning electron microscopy and energy dispersive X-ray spectrometry

Both the external surface as well as sections of young and old biochar particles were observed using SEM. Observations were conducted using a JEOL7600F from the Mica Technology Platform of the Université catholique de Louvain at accelerating voltages of 5 keV and 15 keV and with a working distance of around 10 mm. Before imaging, the samples were coated with a 15-nm gold layer using a Cressington sputter 208HR. From transverse cross-section images, the porosity of biochar was estimated after thresholding using the ImageJ software. The porosity estimated in this way may include pores which are not connected to the outside and therefore reflects total porosity. To identify the presence of mineral matter at the surface of biochar particles, an EDS system which allows the detection of atomic elements was used in conjunction with the SEM. The proportion of atomic elements was obtained using a two-step procedure involving first the subtraction of bremsstrahlung done with the classical "top hat filter" method, and second the quantification of the area under each atomic peak determined by the ZAF model (Osán et al., 2001). ZAF model corrects X-ray intensities for atomic number (Z), absorption (A) and fluorescence (F), ensuring accurate determination of elemental composition in a sample (Maaskant & Kaper, 1991).

2.6 | Soil structure visualization using optical microscopy

The undisturbed soil blocks sampled in polyvinyl chloride boxes were oven-dried (50°C), embedded in an epoxy resin, and then used to manufacture uncovered polished thin sections at the Department of Geology at Ghent University. Thin sections were observed using an optical microscope (Olympus AX70/Provis) from the Mica Technology Platform of the Université catholique de Louvain to assess qualitatively the distribution of biochar particles within the soil samples.

2.7 | Statistical analyses

Data management and analysis were conducted using MATLAB v.2020a software and R studio v.4.0.4. To determine the impact of biochar application on soil physical properties, two-way analyses of variance (ANOVA) were performed using the "aov" function from R studio assuming a randomized complete block design. The "site" factor had two levels (La Bruyère or Attert), whereas the "treatment" factor had four levels (REF, YB1%, YB2%, and OB). Tukey's honestly significant difference post hoc tests (HSD tests) were performed for pairwise comparisons with the "TukeyHSD" function in R studio.

For assessing the relationship between two variables, both "fitlm" and "predict" functions of MATLAB were used to fit a linear model with 95% confidence intervals. To further investigate the correlations between the soil physical properties as well as their relation to soil type, biochar age, and biochar application rate, principal component analysis (PCA) was performed using the "prcomp" and "envfit" functions in R studio.

Whenever applicable, the conditions of homoscedasticity (Levene test) and normality of residuals (visual check using a Q–Q plot and a graph of the residuals distribution) were checked. For this reason, hydraulic conductivity data were log-transformed. Overall, an effect was considered significant when the p-value (P) was less than 0.05. Furthermore, the smoothing function of the Curve Fitting Toolbox in MATLAB was used to smooth the MIP log-transformed differential Hg intrusion volume data in function of the pore size diameter.

3 | RESULTS

3.1 | Soil physical properties

3.1.1 | Bulk density

Based on the ANOVA, there was a significant treatment effect as well as site by treatment interaction on soil bulk density (Table 2). On the silt loam soil, the presence of biochar in YB1%, YB2%, and OB subplots reduced on average the soil bulk density by 14.6%, 18.2%, and 1.5%, respectively, compared to the REF subplots (Table 3). On the sandy loam soil, the soil bulk density decreased by 15.4%, 18.9%, and 12.6% in YB1%, YB2%, and OB subplots, respectively, compared to the REF subplots (Table 3). Soil bulk density was significantly lower in all biochar treatments (YB1%, YB2%, and OB) compared to the reference at both study sites, except for OB on the silt loam soil (Table 3).

Soil bulk density calculated without the direct contribution of biochar was only slightly lower than the uncorrected bulk density ($P < 0.001$). The bulk density values calculated without the direct contribution of biochar were significantly lower in the biochar treatments compared to the reference treatment, except again for the old biochar on the silt loam soil (Table 3).

TABLE 2 Results of analysis of variance (*p*-value) applied to the soil physical characteristics.

Variables	*n*	*p*-values		
		Site	Treatment	Site × treatment
Bulk density	18	0.526	**10^{-15}*****	**0.034***
Bulk density[a]	18	0.515	**10^{-11}*****	**0.036***
Saturated water content	6	**0.037***	**10^{-6}*****	0.224
Macroporosity	6	**0.011***	**10^{-5}*****	0.165
Mesoporosity	6	**0.018***	0.111	0.206
Microporosity	6	**10^{-5}*****	**0.011***	**0.036***
Log(K_s)-HYPROP	6	0.911	**0.019***	**0.029***
Log(K_s)-Inf.	18	**10^{-5}*****	0.327	**0.038***

Note: K_s-HYPROP and K_s-Inf. correspond to the saturated hydraulic conductivity determined using the HYPROP device and the single ring infiltrometer, respectively. Bold values indicate significant effect ($p < 0.05$).

[a]Bulk density calculated without the direct contribution of biochar.

* and *** denote significance at the 0.05 and 0.001probability levels, respectively.

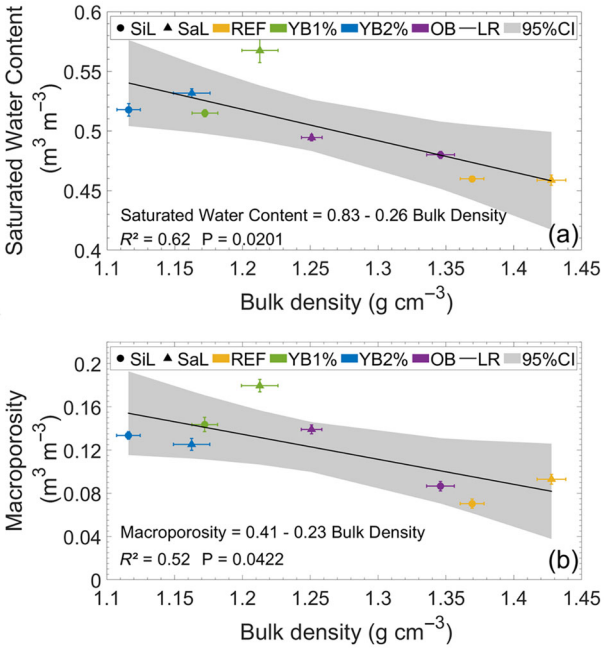

FIGURE 2 Relationship between mean soil bulk density and (a) mean saturated water content or (b) mean macroporosity for the different sites and treatments. SiL and SaL correspond to the silt loam and sandy loam soils, respectively. REF, YB1% and YB2%, and OB correspond to the reference soil, the soil enriched with young biochar at 1% and 2% by weight, and the kiln site soil with old biochar, respectively. The graphs were established by using the same samples for bulk density, saturated water content, and macroporosity ($n = 6$ in all cases). LR and 95% CI correspond to the linear regression line and the 95% confidence interval, respectively. Error bars are standard errors of the means. P corresponds to the *p*-value on the slope parameter of the linear regression.

3.1.2 | Water retention curve and soil pore size distribution

Both site and treatment factors significantly affected the saturated water content (Table 2). On average, across both soils, saturated water content for YB1%, YB2%, and OB was 17.0%, 14.3%, and 6.0% higher, respectively, in relative terms, compared to REF (Table 3). This increase was significant for YB1% and YB2%, but not for OB. However, the measured saturated water content for OB was consistent with the measured bulk densities given the (expected) overall relationship between bulk density and saturated water content (Figure 2a).

While a significant site by treatment interaction was observed for bulk density, the ANOVA did not reveal such an interaction for saturated water content (Table 2), in spite of the strong relationship between both variables (Figure 2a). This lack of significant site by treatment interaction for saturated water content may result from the much lower number of samples for water content ($n = 6$) than for bulk density ($n = 18$). This smaller number of samples may have hampered detection of the site by treatment interaction.

Regarding the water retention curves, compared to the reference subplots, biochar-enriched subplots (OB, YB1%, and YB2%) were characterized by higher water content in the wet end of the retention curve (pF < 1.5; Figure 3). However, as for the saturated water content, the increase in water retention for pF < 1.5 was significant only for YB1% and YB2%. Regarding the OB treatment, water contents were not significantly different from the REF treatment, irrespective of the matric head.

The pore size distributions derived from the water retention curves exhibited a double-hump pattern on both soils (Figure 4). On the silt loam soil, the first peak was located in the macroporosity range between 100 and 200 μm and characterized by a higher magnitude for YB1% and YB2% compared to OB and REF. For the REF treatment, this peak is hardly noticeable. The second higher magnitude peak was located in the mesoporosity range between 4 and 6 μm. On the sandy loam soil, the heterogeneity across the replicates was higher. For the YB1% and YB2% treatments, the highest peak was located in the macroporosity range between 200 and 500 μm, and the second highest magnitude peak was located in the mesoporosity range between 6 and 15 μm. The first peak had a higher magnitude for YB1% compared to YB2%. For OB, soil pore size distribution exhibited a first and second peak at approximately 50 and 2.5 μm, respectively, but the uncertainty (standard errors of the means) was high. The proportion of pores in the REF treatment was of lower or similar magnitude compared to YB1%, YB2%, and OB, irrespective of the pore size.

TABLE 3 Soil physical properties of both study sites for the reference soil (REF), for the soil enriched with young biochar at 1% (YB1%) and 2% (YB2%) by weight and for the kiln site soil with old biochar (OB).

			Silt loam (La Bruyère)				Sandy loam (Attert)			
Variables	**Units**	***n***	**REF**	**YB1%**	**YB2%**	**OB**	**REF**	**YB1%**	**YB2%**	**OB**
Bulk density[a]	g cm^{-3}	18	1.37 ± 0.02a	1.17 ± 0.03b	1.12 ± 0.02b	1.35 ± 0.03a	1.43 ± 0.03a	1.21 ± 0.04b	1.16 ± 0.04b	1.25 ± 0.02b
Bulk density[ab]	g cm^{-3}	18	1.37 ± 0.02a	1.19 ± 0.03b	1.15 ± 0.03b	1.35 ± 0.03a	1.43 ± 0.03a	1.23 ± 0.04b	1.20 ± 0.04b	1.25 ± 0.02b
Saturated water content[c]	m^3 m^{-3}	6	0.460 ± 0.005a	0.515 ± 0.008b	0.518 ± 0.015b	0.480 ± 0.008a	0.459 ± 0.012a	0.567 ± 0.029b	0.532 ± 0.010b	0.494 ± 0.008a
Macroporosity[c]	m^3 m^{-3}	6	0.070 ± 0.012a	0.144 ± 0.019b	0.134 ± 0.010bc	0.087 ± 0.013ac	0.093 ± 0.013a	0.180 ± 0.016b	0.125 ± 0.016bc	0.139 ± 0.012ac
Mesoporosity[c]	m^3 m^{-3}	6	0.284 ± 0.007a	0.279 ± 0.015a	0.293 ± 0.011a	0.285 ± 0.008a	0.238 ± 0.009a	0.279 ± 0.025a	0.288 ± 0.017a	0.246 ± 0.013a
Microporosity[a]	m^3 m^{-3}	6	0.106 ± 0.004a	0.093 ± 0.002a	0.091 ± 0.001a	0.108 ± 0.002a	0.128 ± 0.008a	0.109 ± 0.004a	0.119 ± 0.007a	0.109 ± 0.005a
Log(K_s)-HYPROP[a]	log (mm h^{-1})	6	1.19 ± 0.28a	2.44 ± 0.43a	1.78 ± 0.20a	1.13 ± 0.19a	0.92 ± 0.47a	1.93 ± 0.28a	1.31 ± 0.53a	2.48 ± 0.51a
Log(K_s)-Inf.[a]	log (mm h^{-1})	18	0.98 ± 0.28a	1.38 ± 0.31a	1.63 ± 0.29a	0.76 ± 0.26a	1.70 ± 0.27a	2.16 ± 0.23a	1.85 ± 0.16a	2.48 ± 0.27a

Note: K_s-HYPROP and K_s-Inf. correspond to the saturated hydraulic conductivity determined using the HYPROP device and the single ring infiltrometer, respectively. *n* corresponds to the number of samples. Data are means ± standard errors of the means.

[a]Values followed by different lowercase letters are significantly different according to the site × treatment interaction in the analysis of variance (ANOVA) (Table 2).

[b]Bulk density calculated without the direct contribution of biochar.

[c]Values followed by different lowercase letters are significantly different across treatments, the site × treatment interaction not being significant in the ANOVA (Table 2).

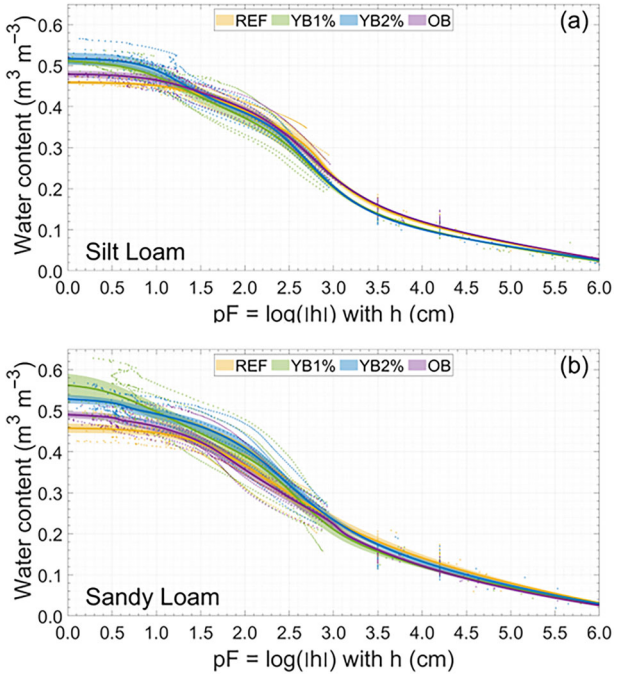

FIGURE 3 Water retention curve for the reference soil (REF), for the soil enriched with young biochar at 1% (YB1%) and 2% (YB2%) by weight, and for the kiln site soil with old biochar (OB) on (a) the silt loam soil (b) the sandy loam soil. Each water retention curve is a mean curve based on six replicates. Points correspond to measurements, shaded areas to the standard errors of the means, and h to the matric head.

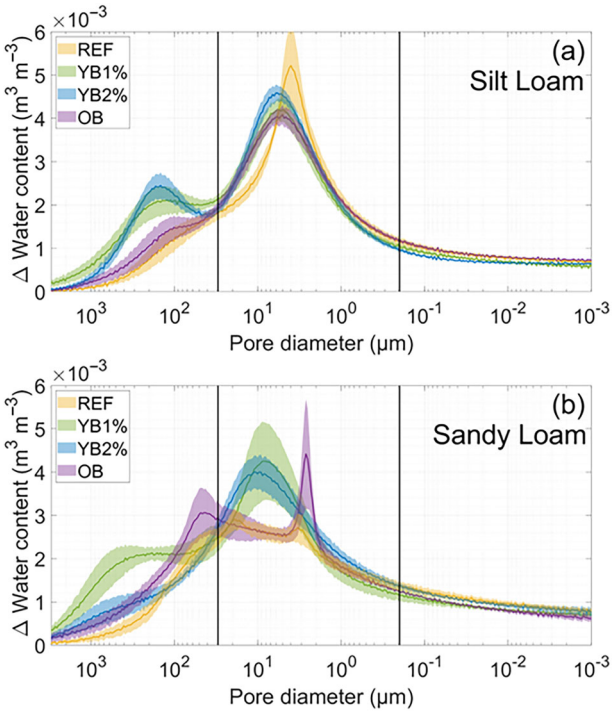

FIGURE 4 Soil pore size distribution derived from the water retention curve for the reference soil (REF), for the soil enriched with young biochar at 1% (YB1%) and 2% (YB2%) by weight, and for the kiln site soil with old biochar (OB) on (a) the silt loam soil (b) the sandy loam soil. Each pore size distribution is a mean curve based on the derivative of the water retention curves. Shaded areas correspond to the standard errors of the means. Black lines correspond to the limit between macroporosity and mesoporosity (30 μm) and between mesoporosity and microporosity (0.2 μm).

For both soils, biochar affected soil macroporosity, but not meso- and microporosity (Table 3). There were significant site and treatment effects on the macroporosity, but no site by treatment interaction (Table 2). Compared to reference soil samples, biochar-enriched soil samples increased the macroporosity by 98.8%, 58.9%, and 38.7%, in relative terms, for YB1%, YB2%, and OB, respectively. This increase was significant for YB1% and YB2%, but not for OB (Table 3). The change in macroporosity for OB was, however, consistent with the observed effect of OB on bulk density as reflected in the overall relationship between macroporosity and bulk density (Figure 2b). Although there was a significant site by treatment interaction for microporosity ($P = 0.036$; Table 2), differences between treatments were small (<2% in absolute value) and no significant difference between the biochar-enriched soils and the reference soils could be identified during pairwise comparison.

3.1.3 | Hydraulic conductivity curve and infiltrometry

For pF < 1.5, there was a tendency for hydraulic conductivity to be higher for biochar-enriched soil samples compared to the reference samples (Figure 5). However, none of the pairwise differences with the reference were significant, which may at least partly result from the high variability observed between replicates from each treatment at both study sites. Moreover, the HYPROP-derived hydraulic conductivity values for pF < 1.5 result from the extrapolation of bimodal Durner models fitted on experimental data which cover a range from pF 1.5 to pF 3, weakening the reliability of these results. For pF > 1.5, there were no differences in hydraulic conductivity values across treatments.

Saturated hydraulic conductivity derived from both HYPROP and infiltrometer measurements is shown in Table 3. Both methodologies tend to indicate that soil samples enriched with young biochar are characterized by higher saturated hydraulic conductivity compared to reference samples, the treatment effect being significant for the saturated hydraulic conductivity derived from HYPROP. The ANOVA also revealed a significant site by treatment interaction (Table 2) for both methodologies. Although none of the pairwise differences with the reference treatment were significant, which may again partly result from the high

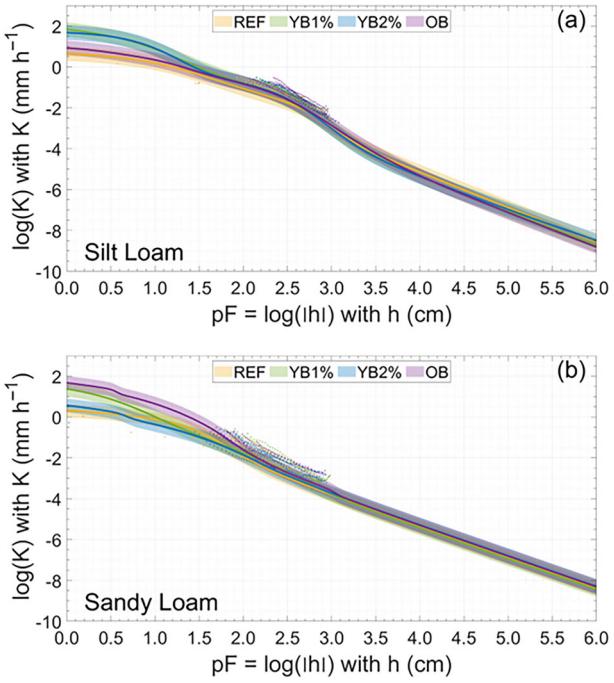

FIGURE 5 Hydraulic conductivity (K) curve for the reference soil (REF), for the soil enriched with young biochar at 1% (YB1%) and 2% (YB2%) by weight, and for the kiln site soil with old biochar (OB) on (a) the silt loam soil (b) the sandy loam soil. Each hydraulic conductivity curve is a mean curve based on six replicates. Points correspond to measurements, shaded areas to the standard errors of the means, and h to the matric head.

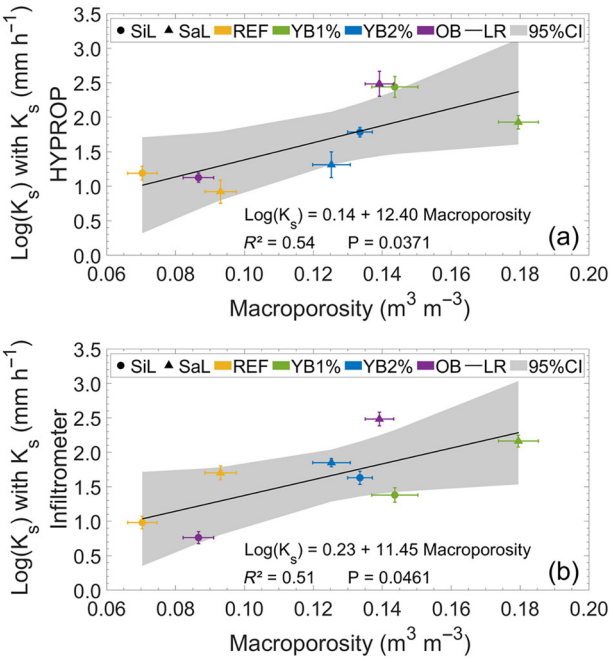

FIGURE 6 Relationship between the macroporosity ($n = 6$) and the logarithm of the saturated hydraulic conductivity (K_s) determined by means of (a) the HYPROP system ($n = 6$) or (b) single ring infiltrometer measurements ($n = 18$). SiL and SaL correspond to silt loam and sandy loam soils, respectively. REF, YB1% and YB2%, and OB correspond to the reference soil, the soil enriched with young biochar at 1% and 2% by weight, and the kiln site soil with old biochar, respectively. LR and 95% CI correspond to the linear regression line and the 95% confidence interval, respectively. Error bars are standard errors of the means. P corresponds to the *p*-value on the slope parameter of the linear regression.

variability observed between the replicate measurements for each treatment (Table 3), this significant interaction seems to result mostly from the contrasted effect of OB at both sites. While OB has no or even a slightly negative impact on the saturated hydraulic conductivity on the silt loam soil, its effect on the sandy loam soil is positive and rather large.

Whatever the measurement methodology (HYPROP or infiltrometer), the saturated hydraulic conductivity was significantly correlated to the macroporosity (Figure 6). Given that macroporosity was significantly affected by the addition of young biochar to soil (Table 3), these correlations are an additional indication that addition of biochar increases saturated hydraulic conductivity.

3.1.4 | Principal component analysis

Figure 7 displays the results of the PCA performed on the soil physical properties. The first and second components of the PCA explained 42.3% and 25.1% of the total variance in the dataset, respectively. The first principal component is strongly correlated with the bulk density ($r = -0.89$), the saturated water content ($r = 0.70$), the macroporosity ($r = 0.93$), as well as the logarithm of saturated hydraulic conductivity measured by means of the HYPROP system ($r = 0.70$). It is moderately correlated with the microporosity ($r = -0.53$). The second principal component is strongly correlated with the mesoporosity ($r = -0.96$), and moderately correlated with the saturated water content ($r = -0.52$), the logarithm of saturated hydraulic conductivity measured by means of the HYPROP system ($r = 0.49$) and by means of the single ring infiltrometer ($r = 0.43$). Both components do not discriminate between silt loam and sandy loam soils (P = 0.15), but discriminate well between the different treatments (P = 0.001), except between the YB1% and YB2% treatments. The OB cluster has an intermediate location between the young biochar (YB1% and YB2%) clusters and the REF cluster.

3.1.5 | Helium pycnometry and mercury intrusion porosimetry

Table 4 and Figure 8 show the characteristics of the biochar pore network derived from the helium pycnometry and MIP

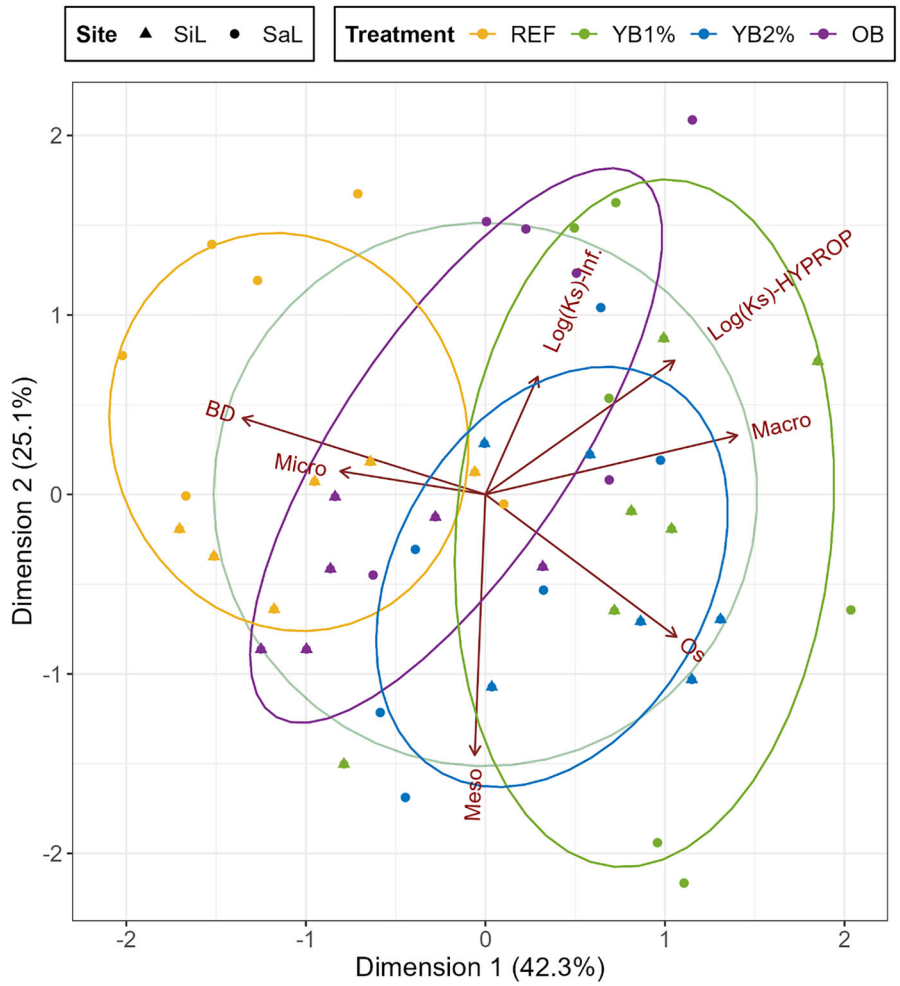

FIGURE 7 Superimposition of the maps of variables (purple arrows), individuals (markers), and clusters (ovals) from the principal component analysis (PCA) performed on the soil physical properties. BD, Os, Macro, Meso, Micro, and Log(Ks)-HYPROP and Log(Ks)-Inf correspond to the bulk density ($n = 6$), the saturated water content ($n = 6$), the macroporosity ($n = 6$), the mesoporosity ($n = 6$), the microporosity ($n = 6$), and the logarithmic saturated hydraulic conductivity measured by means of the HYPROP system ($n = 6$) and the single ring infiltrometer ($n = 18$), respectively. Regarding soil bulk density, only the measurements performed on the same sample as those used for determining the water retention curve and derived parameters were considered. SiL and SaL correspond to silt loam and sandy loam soils, respectively. REF, YB1% and YB2%, and OB correspond to the reference soil, the soil enriched with young biochar at 1% and 2% by weight, and the kiln site soil with old biochar, respectively.

measurements. Particle density was not significantly different for young and old biochar, whereas bulk density was lower for young biochar compared to old biochar. Young biochar was characterized by higher porosity compared to old biochar. The young biochar particles exhibited a bimodal pore size distribution with a predominant mode at 12.4 μm and a second lower magnitude peak at 1.5 μm (Figure 8). The old biochar particles were characterized by a very low accessible porosity (<15%). The median pore diameter of young biochar was about an order of magnitude higher than the old biochar (Table 4).

3.1.6 | Scanning electron microscopy and energy dispersive X-ray spectrometry

Based on the transverse cross-section images of biochar particles taken with the SEM (Figure 9 a,c,e), the total porosity of the young biochar particles was 15% higher (in absolute terms) than the porosity of the old biochar from the kiln sites for both soils (Table 4). For the young biochar particles, the pore diameter was mostly in the range from 20 to 40 μm and corresponds to the tracheids of the pyrolyzed wood (*Picea abies*). For the old biochar particles, the observations

TABLE 4 Biochar pore network characteristics derived from the helium pycnometry, mercury intrusion porosimetry, and scanning electron microscopy (SEM) observation.

	Helium pycnometry and mercury intrusion porosimetry				SEM
	Particle density (g cm^{-3})	Bulk density (g cm^{-3})	Porosity (m^3 m^{-3})	Median pore diameter (μm)	Porosity (m^3 m^{-3})
Biochar type	***n* = 3**	***n* = 3**	***n* = 3**	***n* = 3**	***n* = 3**[a]
Young biochar	1.09 ± 0.10a	0.45 ± 0.03a	0.59 ± 0.03a	12.4 ± 0.4a	0.57 ± 0.04a
Old biochar-SiL	1.09 ± 0.06a	0.99 ± 0.04b	0.09 ± 0.03b	1.2 ± 0.1b	0.42 ± 0.02b
Old biochar-SaL	1.25 ± 0.01a	1.09 ± 0.01b	0.13 ± 0.01b	1.9 ± 0.0c	0.42 ± 0.02b

Note: SiL and SaL correspond to the silt loam and sandy loam soils, respectively. Data are means ± standard errors of the means.
[a]Three samples for each type of biochar, but for each sample two–five SEM images were analyzed.

FIGURE 8 Pore size distribution of (a) the young biochar, (b) the old biochar from the silt loam (SiL) soil, and (c) the old biochar from the sandy loam (SaL) soil, derived from mercury intrusion porosimetry measurements. Each distribution is a mean curve based on three replicates. Points correspond to the measurements and shaded areas to the standard errors of the means.

of the transverse cross-section images revealed a bimodal pore size distribution with vessel elements approximately 40 μm in diameter and labriform fibers approximately 10 μm in diameter.

Figure 10 shows the proportion of atomic elements detected with the EDS system. The carbon content was high, and the O:C ratio was low both at the surface and inside the young biochar particles. For the old biochar, the O:C ratio was high at the surface of the particles and low inside the particles. Moreover, aluminum and silicon elements were detected at the surface of the old biochar but not on the young biochar, suggesting the presence of soil particles at the surface of the old biochar. The presence of clay and silt particles on the surface of the old biochar was confirmed visually by means

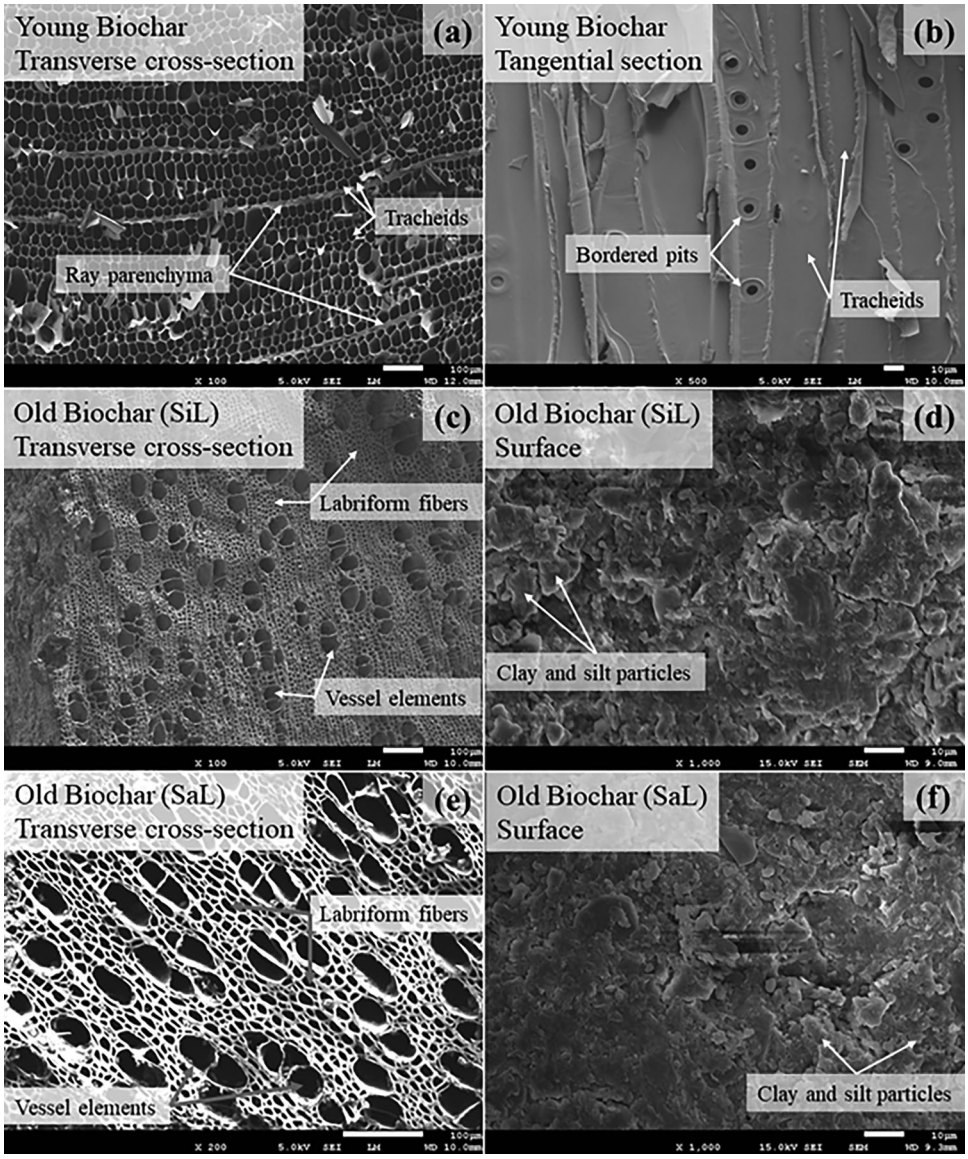

FIGURE 9 Scanning electron microscopy (SEM) images of biochar particles. Transverse cross-section (a,c,e), tangential section (b), and external surface (d,f) of the young biochar (a,b) and old biochar from the silt loam (SiL) soil (c,d) and sandy loam (SaL) soil (e,f).

of the SEM images of the surface of the old biochar particles (Figure 9d,f).

4 | DISCUSSION

4.1 | Biochar effects on soil physical properties

Prior to the experiments, it was hypothesized that biochar addition to soils would improve the soil physical properties. Based on the results, it appears that burying young biochar in soil indeed improved the physical properties overall, at both study sites. The addition of young biochar to soil reduced the bulk density, increased macroporosity and consequently water content on the wet end of the retention curve (pF < 1.5), and tended to increase the saturated hydraulic conductivity (Table 3). Such improvements in soil physical properties following the application of biochar are consistent with the literature. The meta-analyses of Omondi et al. (2016), Razzaghi et al. (2020), and Singh et al. (2022) reported a reduction in soil bulk density by 8%, 9%, and 29% on average, respectively. The review of Blanco-Canqui (2017) reported a relative increase in total porosity by 14%–64% following biochar addition, which is consistent with the increase in saturated water content observed in the present study, saturated water content being a measure of total accessible soil porosity. Even though Hardie et al. (2014) and Petersen et al. (2016) did not report an effect of biochar on soil macroporosity, greater macroporosity in biochar-enriched

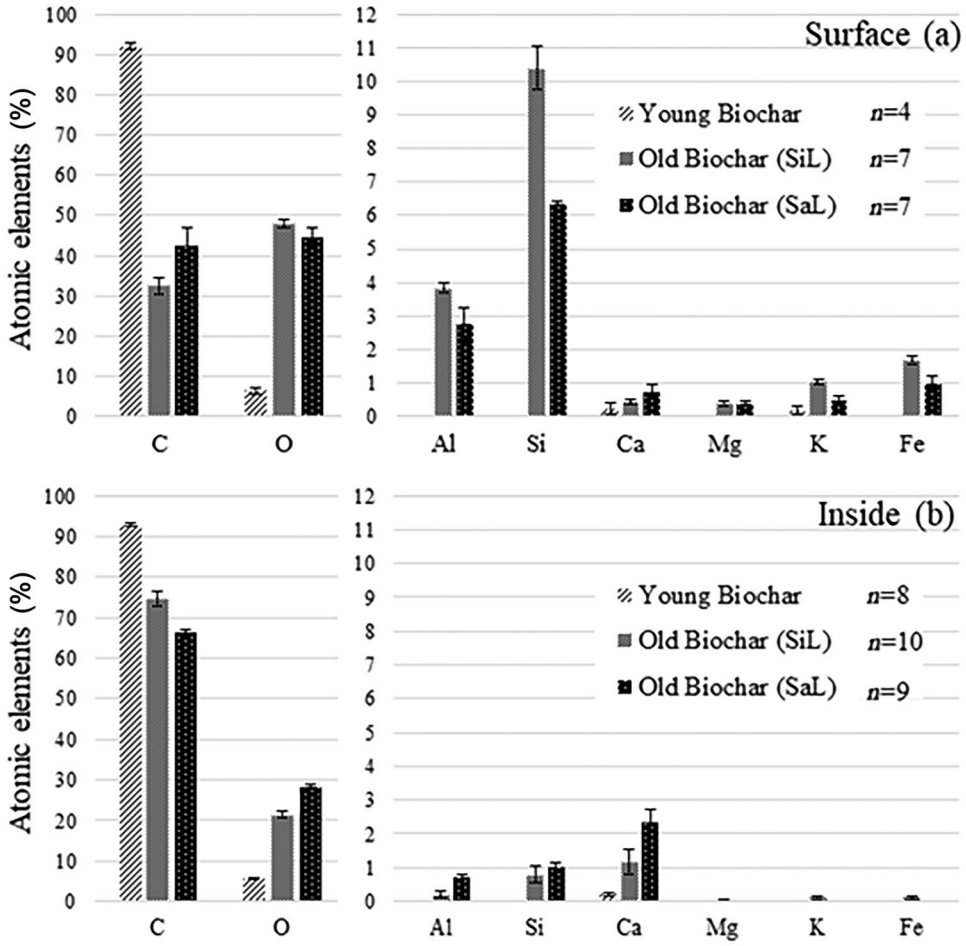

FIGURE 10 Proportion of atomic elements detected with the energy dispersive X-ray spectrometer mounted on the scanning electron microscope (a) at the external surface of and (b) inside biochar particles. Data are means ± standard errors of the means. Zero was attributed to values below detection limit. SiL and SaL correspond to the silt loam soil and the sandy loam soil, respectively.

soils was observed by Herath et al. (2013) and Sun et al. (2013), as in the present study. Consistent with the trend in the present study, the meta-analysis of Omondi et al. (2016) reported an increase in saturated hydraulic conductivity. However, we did not observe a texture-dependent effect of biochar on saturated hydraulic conductivity, as reported, for instance, in the review of Blanco-Canqui (2017) and the meta-analysis of Edeh et al. (2020). These two reviews have shown that saturated hydraulic conductivity decreases in coarse-textured soils, is unaffected in medium-textured soils and increases in fine-textured soils following the addition of biochar. Also not observed in the present study are the increases in mesoporosity (i.e., plant available water capacity) and microporosity highlighted by the meta-analysis of Razzaghi et al. (2020).

Regarding the effect of biochar application rate, we expected that the positive effects on soil physical properties would increase with increasing biochar application rates. Indeed, existing meta-analyses often indicate that biochar application rate has a positive impact on soil water properties (Omondi et al., 2016). Nevertheless, some previous meta-analyses suggest that improvements in soil physical properties are greatest for intermediate biochar application rates. For example, the meta-analysis of Edeh et al. (2020) revealed that biochar application was most effective in improving soil water properties with application rates between 30 and 70 Mg ha^{-1}. In the present study, however, the effects of biochar content were inconsistent. The limited differences in soil physical properties between the 2% biochar samples and 1% biochar samples might imply the existence of a biochar content threshold, although the underlying mechanisms remain to be elucidated.

Finally, we hypothesized that biochar fragmentation and aging processes could strengthen the impact of biochar on soil physical properties. On the one hand, biochar fragmentation results in an increase in external surface of biochar particles in contact with the soil constituents. On the other hand, biochar aging increases its cation exchange capacity and, consequently, soil exchangeable Ca^{2+} and Mg^{2+} contents (Hardy et al., 2016). This could enhance the role of biochar as

binding agent in organo-mineral associations and strengthen the impact of biochar on soil structure (Burgeon et al., 2021). However, the presence of century-old biochar particles in kiln sites did not significantly affect the soil physical properties at both study sites, except for the bulk density on the sandy loam soil (Table 3). The lack of significant effect could in part be due to the lower biochar content in kiln sites (0.6%–0.7%) compared to young biochar treatments (1%–2%). Nevertheless, the values of the measured soil physical properties for the old biochar treatment often lie in-between the values for the young biochar and the reference treatments (Figure 2). This is also apparent in the PCA (Figure 7). The presence of century-old biochar in kiln sites may thus slightly improve soil physical properties, though not sufficiently to achieve a significant effect. Yet there is no indication that biochar aging and fragmentation have enhanced the capacity of biochar to improve soil structure compared to young biochar. Some caution is, however, warranted regarding the comparison between the young and old biochar treatments. Indeed, besides the differences in concentration, the differences in the type of feedstock and conditions of production between the young and old biochar may also affect the intensity of soil response to biochar additions (Gholamahmadi et al., 2023; Islam et al., 2021; Singh et al., 2022).

4.2 | Mechanisms of biochar impact

Since some soil properties were positively affected by biochar additions, what could explain the observed changes? Biochar addition to soil can affect the soil pore network through its internal porous system (Brewer et al., 2014; Hyväluoma et al., 2018; Lehmann & Joseph, 2009; Yi et al., 2020) as well as through its location in the soil structure and interaction with the soil constituents. Regarding the latter, biochar particles can fill and clog the voids in between the mineral grains, especially in coarse-textured soils (Edeh et al., 2020), take up space previously occupied by mineral particles or organo-mineral micromass, or improve soil structure and soil aggregation by acting as an additional binding agent in the soil (Burgeon et al., 2021; Du et al., 2017). This latter mechanism is similar to the aggregating effect of uncharred organic matter and it cannot be dissociated from an indirect impact of biochar on uncharred organic matter (Burgeon et al., 2021; Hardy et al., 2016; Hernandez-Soriano et al., 2015; Kerré et al., 2016) or on soil biology (Li et al., 2020; Wang et al., 2023; Zhang et al., 2018).

4.3 | Internal porosity of biochar particles

Regarding the young biochar, the reduction in soil bulk density and the increase in macroporosity can be explained to a limited extent only by the internal porosity of biochar. First, the low density of biochar explains only a minor part of the observed reduction in soil bulk density following the application of biochar. Indeed, the soil bulk density calculated without the direct contribution of young biochar particles remained noticeably lower than the soil bulk density of the reference samples. This indicates that the low density of biochar cannot by itself explain the lower bulk density of biochar-enriched soils. Second, the increase in macroporosity following the addition of biochar cannot be attributed to the porosity of biochar. Indeed, although most of its porosity consists of tracheids between 20 and 40 μm in diameter (the limit between meso- and macropores), these tracheids are not continuous but connected to each other via bordered pits which control the sap flow in conifer wood such as *Picea abies* (Choat et al., 2008; Figure 9b). These bordered pits have a smaller diameter than tracheids and are expected to control the emptying of the latter. The pore sizes derived from the SEM images are therefore not directly comparable to pore size distributions derived from water retention curves because SEM-derived pore sizes do not take into account the connectivity between pores. In that respect, pore size distributions derived from MIP are more comparable to pore size distributions derived from water retention curves. According to MIP and the assumptions underlying the methodology (e.g., Hg–soil contact angle), the porosity of young biochar particles is dominated by pores in the 5–30 μm range (Figure 8). These pore sizes are smaller than the ones affected by the application of biochar (50–2000 μm for a water–soil contact angle $\beta = 0°$; Figure 4). Note that this outcome is not significantly affected by the choice of soil–water contact angle in the range 0°–60°. Hence, for the soils investigated in this study, the impact of biochar application on soil macroporosity cannot be explained to a significant extent by the internal porosity of fresh biochar particles themselves.

Regarding the old biochar in kiln sites, the effects on soil physical properties were mostly nonsignificant, and, consequently, one can deduce that the biochar pore network characteristics also had a limited effect. Furthermore, the total porosity measured with MIP was much lower than the total porosity estimated with the SEM transverse cross-section image analyses. The difference in total porosity determined with both methods indicates that the porosity of the old biochar was not accessible. Our hypothesis is that the coating of the old biochar surface by clay particles, as observed with the SEM and confirmed by atomic element detection (Figures 9 and 10), did not allow Hg to enter into the porosity inside the old biochar particles. In other words, we suggest that the internal porosity of old biochar particles was not accessible due to the adsorption of clay particles and the clogging of pores at the surface of the old biochar. The coating of the surface of aged biochar particles by clay particles, in addition to the occlusion of biochar pores by these clay

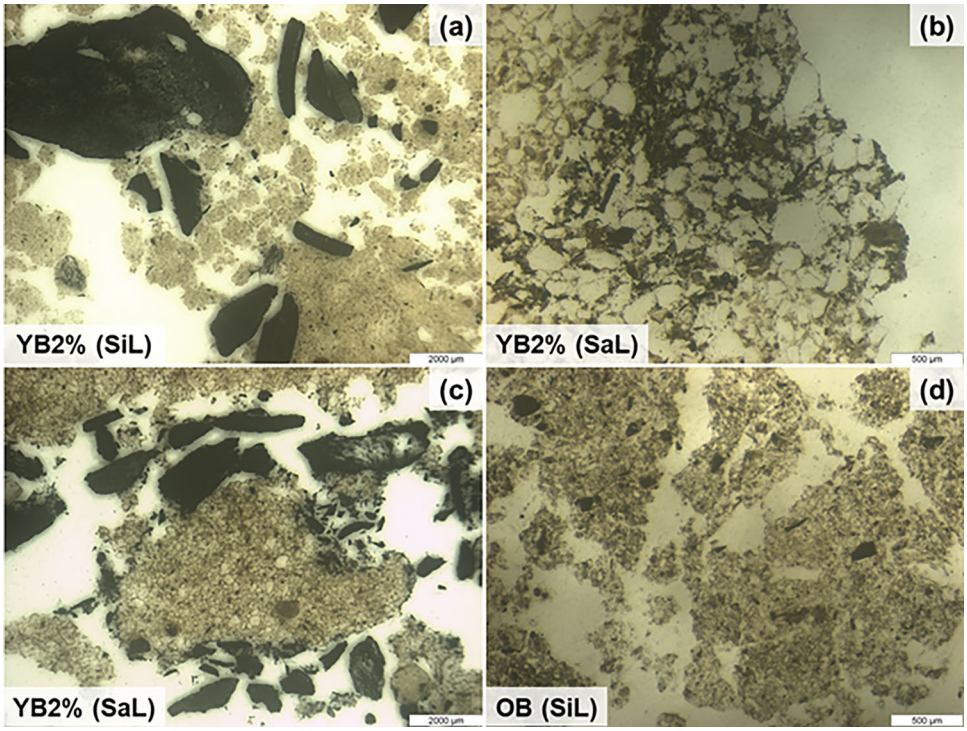

FIGURE 11 Illustration of the location of biochar particles within soil aggregates, on the outer edge of soil aggregates and within soil porosity. SiL and SaL correspond to the silt loam and sandy loam soil, respectively. YB2% and OB correspond to the soil enriched with young biochar at 2% by weight and century-old biochar in kiln sites, respectively.

particles, were already observed by Hardy et al. (2017) in kiln sites. Even if the internal porosity were accessible, the total porosity of the old biochar particles as derived from SEM (Table 4) is lower than the total porosity of the reference soil (using saturated water content as a proxy of total porosity; Table 3). Hence, as opposed to the young biochar used in the present study, old biochar particles could not possibly increase the total soil porosity by means of their internal porosity.

4.4 | Biochar location and interaction with soil

Besides the direct contribution of their internal porosity, biochar particles may also affect the soil pore network depending on their distribution in the soil and their interaction with the soil components. In the present study, there is no evidence of a net clogging effect following biochar addition, that is, no filling of voids in between mineral grains or aggregates. Indeed, this would have resulted in a higher soil bulk density, a lower porosity, and a lower saturated hydraulic conductivity in biochar-amended soil compared to the reference soil. On the contrary, addition of biochar resulted in a structuring effect, as supported by the improvement of several soil physical properties in biochar-enriched soils compared to reference soils (Table 3).

Optical microscopy observations on undisturbed soil thin sections revealed that both young and old biochar particles were present in soil as isolated single particles or located within and at the surface of soil aggregates (Figure 11a–d). The presence of young biochar within soil aggregates was also observed using optical microscopy by Jien and Wang (2013), Prakongkep et al. (2020), and Zhang et al. (2020). The location of biochar particles within aggregates and at the surface of aggregates suggests that biochar may play an active role in soil structure formation and stabilization due to its surface charges. Actually, the location of biochar particles within soil tended to differ depending on the particle size of biochar. The biggest particles were preferentially present as single particles, whereas the finest particles were preferentially located within soil aggregates or at their surface. This suggests that finer biochar particles could contribute more to soil structure improvement than larger biochar particles. The greater impact of finer biochar particles on soil structure could be explained by their higher external surface in contact with soil constituents, compared to larger biochar particles.

5 | CONCLUSIONS

In the present study, we hypothesized that amending soils with biochar may improve soil physical properties, but that the magnitude of these changes would depend on the

application rate and biochar aging. At both study sites, it was found that fresh biochar application to soil decreased the bulk density and increased both the water content near saturation (pF < 1.5) and macroporosity. However, no consistent effect of biochar application rate was observed. It was shown that the improvement of soil physical properties in the short-term appears related to the improvement of soil structure rather than to the internal porosity of the biochar particles. Regarding the effect of biochar aging, soil physical properties were mostly not significantly different for soil samples containing century-old biochar at kiln sites compared to samples with no added biochar. This could be related to the low biochar content in kiln sites, but also to the mostly inaccessible internal porosity of old biochar particles as a result of the clogging of pores by clay particles. The results also appear to indicate that biochar fragmentation and surface oxidation during aging do not strongly enhance its ability to improve soil structure, at least when considering biochar that is more than a century old. It would therefore be of interest to investigate the effects of biochar on soil physical properties over intermediate time scales by means of long-term trials.

AUTHOR CONTRIBUTIONS

Martin Zanutel: Conceptualization; data curation; formal analysis; funding acquisition; investigation; methodology; resources; software; validation; visualization; writing—original draft. **Sarah Garré**: Conceptualization; supervision; validation. **Patrick Sanglier**: Investigation. **Charles Bielders**: Conceptualization; funding acquisition; methodology; supervision; validation; writing—original draft.

ACKNOWLEDGMENTS

This work is part of a Ph.D. supported by a FRIA grant from the Belgian Fund for Scientific Research (FSR-FNRS). The authors would like to thank Mr. Jan Jurceka and Prof. De Grave from the department of Geology in Ghent University for the preparation of soil thin sections. The authors would like to thank Ms. Delphine Magnin and the Mica Technology Platform from the Université catholique de Louvain for access to and assistance with the optical and electron microscopes. The authors would also like to thank Prof. Vincke from the Université catholique de Louvain for the help in the understanding of SEM images of biochar samples.

CONFLICT OF INTEREST STATEMENT

The authors declare no conflicts of interest.

ORCID

Martin Zanutel https://orcid.org/0000-0002-6924-0649
Sarah Garré https://orcid.org/0000-0001-9025-5282
Patrick Sanglier https://orcid.org/0000-0001-5976-5903

REFERENCES

Abiven, S., Menasseri, S., & Chenu, C. (2009). The effects of organic inputs over time on soil aggregate stability—A literature analysis. *Soil Biology & Biochemistry*, *41*, 1–12. https://doi.org/10.1016/j.soilbio.2008.09.015

Andrenelli, M. C., Maienza, A., Genesio, L., Miglietta, F., Pellegrini, S., Vaccari, F. P., & Vignozzi, N. (2016). Field application of pelletized biochar: Short term effect on the hydrological properties of a silty clay loam soil. *Agricultural Water Management*, *163*, 190–196. https://doi.org/10.1016/j.agwat.2015.09.017

Anton Paar. (2023). *Semi-solid and solid density analyzers*. Anton Paar. https://www.anton-paar.com/?eID=documentsDownload&document=70931&L=

Berhane, M., Xu, M., Liang, Z., Shi, J., Wei, G., & Tian, X. (2020). Effects of long-term straw return on soil organic carbon storage and sequestration rate in North China upland crops: A meta-analysis. *Global Change Biology*, *26*, 2686–2701. https://doi.org/10.1111/gcb.15018

Blanco-Canqui, H. (2017). Biochar and soil physical properties. *Soil Science Society of America Journal*, *81*, 687–711. https://doi.org/10.2136/sssaj2017.01.0017

Blanco-Canqui, H. (2021). Does biochar application alleviate soil compaction? Review and data synthesis. *Geoderma*, *404*, 115317. https://doi.org/10.1016/j.geoderma.2021.115317

Borchard, N., Siemens, J., Ladd, B., Möller, A., & Amelung, W. (2014). Application of biochars to sandy and silty soil failed to increase maize yield under common agricultural practice. *Soil & Tillage Research*, *144*, 184–194. https://doi.org/10.1016/j.still.2014.07.016

Boyle, M., Frankenberger, W. T., & Stolzy, L. H. (1989). The influence of organic matter on soil aggregation and water infiltration. *Journal of Production Agriculture*, *2*, 209–299. https://doi.org/10.2134/jpa1989.0290

Brewer, C. E., Chuang, V. J., Masiello, C. A., Gonnermann, H., Gao, X., Dugan, B., Driver, L. E., Panzacchi, P., Zygourakis, K., & Daviese, C. (2014). New approaches to measuring biochar density and porosity. *Biomass and Bioenergy*, *66*, 176–185. https://doi.org/10.1016/j.biombioe.2014.03.059

Burgeon, V., Fouché, J., Garré, S., Dekhordi, R. H., Colinet, G., & Cornelis, J.-T. (2022). Young and century-old biochars strongly affect nutrient cycling in a temperate agroecosystem. *Agriculture, Ecosystems & Environment*, *328*, 107847. https://doi.org/10.1016/j.agee.2021.107847

Burgeon, V., Fouché, J., Leifeld, J., Chenu, C., & Cornelis, J.-T. (2021). Organo-mineral associations largely contribute to the stabilization of century-old pyrogenic organic matter in cropland soils. *Geoderma*, *388*, 114841. https://doi.org/10.1016/j.geoderma.2020.114841

Choat, B., Cobb, A. R., & Jansen, S. (2008). Structure and function of bordered pits: New discoveries and impacts on whole-plant hydraulic function. *New Phytologist*, *177*, 608–626. https://doi.org/10.1111/j.1469-8137.2007.02317.x

De Stephano, A., & Jacobson, M. G. (2017). Soil carbon sequestration in agroforestry systems: A meta-analysis. *Agroforestry Systems*, *92*, 285–299. https://doi.org/10.1007/s10457-017-0147-9

Doerr, S. H. (1998). On standardizing the "water drop penetration time" and the "molarity of an ethanol droplet" techniques to classify soil hydrophobicity: A case study using medium textured soils. *Earth Surface Processes and Landforms*, *23*, 663–668. https://doi.org/10.1002/(SICI)1096-9837(199807)23:73.0.CO;2-6

Du, Z.-L., Zhao, J.-K., Wang, Y.-D., & Zhang, Q.-Z. (2017). Biochar addition drives soil aggregation and carbon sequestration in aggregate fractions from an intensive agricultural system. *Journal of Soils and Sediments*, *17*, 581–589. https://doi.org/10.1007/s11368-015-1349-2

Durner, W. (1994). Hydraulic conductivity estimation for soils with heterogeneous pore structure. *Water Resources Research*, *30*, 211–223. https://doi.org/10.1029/93WR02676

European Commission (EC). (2006). *Communication from the Commission to the Council, the European Parliament, the European Economic and Social Committee of the Regions, thematic strategy for soil protection*. https://eur-lex.europa.eu/LexUriServ/LexUriServ.do?uri=COM:2006:0231:FIN:EN:PDF

Edeh, I. G., Mašek, O., & Buss, W. (2020). A meta-analysis on biochar's effects on soil water properties—New insights and future research challenges. *Science of the Total Environment*, *714*, 136857. https://doi.org/10.1016/j.scitotenv.2020.136857

Gardner, W. R. (1958). Some steady-state solutions of the unsaturated moisture flow equation with application to evaporation from a water table. *Soil Science*, *85*, 228–232. https://doi.org/10.1097/00010694-195804000-00006

Gholamahmadi, B., Jeffery, S., Gonzalez-Pelayo, O., Prats, S. A., Bastos, A. C., Keizer, J. J., & Verheijen, F. G. A. (2023). Biochar impacts on runoff and soil erosion by water: A systematic global scale meta-analysis. *Science of the Total Environment*, *871*, 161860. https://doi.org/10.1016/j.scitotenv.2023.161860

Goidts, E., & van Wesemael, B. (2007). Regional assessment of soil organic carbon changes under agriculture in southern Belgium (1955–2005). *Geoderma*, *141*, 341–354. https://doi.org/10.1016/j.geoderma.2007.06.013

Gurwick, N. P., Moore, L. A., Kelly, C., & Elias, P. (2013). A systematic review of biochar research, with a focus on its stability in situ and its promise as a climate mitigation strategy. *PLoS ONE*, *8*, e75932. https://doi.org/10.1371/journal.pone.0075932

Hardie, M., Clothier, B., Bound, S., Oliver, G., & Close, D. (2014). Does biochar influence soil physical properties and soil water availability? *Plant and Soil*, *376*, 347–361. https://doi.org/10.1007/s11104-013-1980-x

Hardy, B., Cornélis, J.-T., Houben, D., Leifeld, J., Lambert, R., & Dufey, J. E. (2016). Evaluation of the long-term effect of biochar on properties of temperate agricultural soil at pre-industrial charcoal kiln sites in Wallonia, Belgium. *European Journal of Soil Science*, *68*, 80–89. https://doi.org/10.1111/ejss.12395

Hardy, B., & Dufey, J. (2015). Kiln sites in walloon forest: Location, morphology and spatial distribution. *Forêt Nature*, *135*, 20–30. (In French).

Hardy, B., Leifeld, J., Knicker, H., Dufey, J. E., Deforce, K., & Cornélis, J.-T. (2017). Long term change in chemical properties of preindustrial charcoal particles aged in forest and agricultural temperate soil. *Organic Geochemistry*, *107*, 33–45. https://doi.org/10.1016/j.orggeochem.2017.02.008

Hardy, B., Sleutel, S., Dufey, J. E., & Cornelis, J.-T. (2019). The long-term effect of biochar on soil microbial abundance, activity and community structure is overwritten by land management. *Frontiers in Environmental Science*, *7*, 110, https://doi.org/10.3389/fenvs.2019.00110

Herath, H. M. S. K., Camps-Arbestain, M., & Hedley, M. (2013). Effect of biochar on soil physical properties in two constrasting soils: An Alfisol and an Andisol. *Geoderma*, *209–210*, 188–197. https://doi.org/10.1016/j.geoderma.2013.06.016

Hernandez-Soriano, M. C., Kerré, B., Goos, P., Hardy, B., Dufey, J., & Smolders, E. (2015). Long-term effect of biochar on the stabilization of recent carbon: Soils with historical inputs of charcoal. *GCB Bioenergy*, *8*, 371–381. https://doi.org/10.1111/gcbb.12250

Hyväluoma, J., Kuljun, S., Hannula, M., Wikberg, H., Källi, A., & Rasa, K. (2018). Quantitative characterization of pore structure of several biochars with 3D imaging. *Environmental Science and Pollution Research*, *25*, 25648–25658. https://doi.org/10.1007/s11356-017-8823-x

Islam, M. U., Jiang, F., Guo, Z., & Peng, X. (2021). Does biochar application improve soil aggregation? A meta-analysis. *Soil & Tillage Research*, *209*, 104926. https://doi.org/10.1016/j.still.2020.104926

Jeffery, S., Meinders, M. B. J., Stoof, C. R., Bezemer, T. M., van de Voorde, T. F. J., Mommer, L., & van Groenigen, J. W. (2015). Biochar application does not improve the soil hydrological function of a sandy soil. *Geoderma*, *251–252*, 47–54. https://doi.org/10.1016/j.geoderma.2015.03.022

Jien, S.-H., & Wang, C.-S. (2013). Effects of biochar on soil properties and erosion potential in a highly weathered soil. *Catena*, *110*, 225–233. https://doi.org/10.1016/j.catena.2013.06.021

Juriga, M., & Šimanský, V. (2018). Effect of biochar on soil structure—A review. *Acta fytotechnica et zootechnica*, *21*, 11–19. https://doi.org/10.15414/afz.2018.21.01.11-19

Kerré, B., Bravo, C. T., Leifeld, J., Cornelissen, G., & Smolders, E. (2016). Historical soil amendment with charcoal increases sequestration of non-charcoal carbon: A comparison among methods of black carbon quantification. *European Journal of Soil Science*, *67*, 324–331. https://doi.org/10.1111/ejss.12338

Kerré, B., Willaert, B., Cornelis, Y., & Smolders, E. (2017). Long-term presence of charcoal increases maize yield in Belgium due to increased soil water availability. *European Journal of Agronomy*, *91*, 10–15. https://doi.org/10.1016/j.eja.2017.09.003

Kerré, B., Willaert, B., & Smolders, E. (2017). Lower residue decomposition in historically charcoal-enriched soils is related to increased adsorption of organic matter. *Soil Biology and Biochemistry*, *104*, 1–7. https://doi.org/10.1016/j.soilbio.2016.10.007

Klock, G. O., Boersma, L., & De Backer, L. W. (1969). Pore size distributions as measured by the mercury intrusion method and their use in predicting permeability. *Soil Science Society of America Journal*, *33*, 12–15. https://doi.org/10.2136/sssaj1969.03615995003300010009x

Kong, A. Y. Y., Six, J., Dennis, C., Bryant, R., Denison, R. F., & van Kessel, K. (2005). The relationship between carbon input, aggregation, and soil organic carbon stabilization in sustainable cropping systems. *Soil Science Society of America Journal*, *69*, 1078–1085. https://doi.org/10.2136/sssaj2004.0215

Lawrence, G. P. (1977). Measurement of pore sizes in fine-textured soils: A review of existing techniques. *Journal of Soil Science*, *28*, 527–540.

Lee, M.-H., Chang, E.-H., Lee, C.-H., Chen, J.-Y., & Jien, S.-H. (2021). Effects of biochar on soil aggregation and distribution of organic carbon fractions in aggregates. *Processes*, *9*, 1431. https://doi.org/10.3390/pr9081431

Lehmann, J., Cowie, A., Masiello, C. A., Kammann, C., Woolf, D., Amonette, J. E., Cayuela, M. L., Camps-Arbestain, M., & Whitman, T. (2021). Biochar in climate change mitigation. *Nature Geoscience*, *14*, 883–892. https://doi.org/10.1038/s41561-021-00852-8

Lehmann, J., & Joseph, S. (2009). *Biochar for environmental management: Science and technology*. Earthscan.

Li, X., Wang, T., Chang, S. X., Jiang, X., & Song, Y. (2020). Biochar increases soil microbial biomass but has variable effects on microbial

diversity: A meta-analysis. *Science of The Total Environment*, *749*, 141593. https://doi.org/10.1016/j.scitotenv.2020.141593

Li, X., & Zhang, L. M. (2009). Characterization of dual-structure pore-size distribution of soil. *Canadian Geotechnical Journal*, *46*, 129–141. https://doi.org/10.1139/T08-110

Luo, Z., Wang, E., & Sun, O. J. (2010). Can no-tillage stimulate carbon sequestration in agricultural soils? A meta-analysis of paired experiments. *Agriculture, Ecosystems & Environment*, *139*, 224–231. https://doi.org/10.1016/j.agee.2010.08.006

Maaskant, P., & Kaper, H. (1991). Fluorescence effects at phase boundaries: petrological implications for Fe-Ti oxides. *Mineralogical Magazine*, *55*(379), 277–279. https://doi.org/10.1180/minmag.1991.055.379.16

METER Group. (2018). *WP4C: Dew Point PotentiaMeter* (operator's manual). Decagon Devices, Inc.

Mia, S., Dijkstra, F. A., & Singh, B. (2017). Chapter one—Long-term aging of biochar: A molecular understanding with agricultural and environmental implications. *Advances in Agronomy*, *141*, 1–51. https://doi.org/10.1016/bs.agron.2016.10.001

Micromeritics. (2017). *AutoPore IV operator manual*. Micromeritics Instrument Corporation.

Muñoz-Castelblanco, J. A., Pereira, J. M., Delage, P., & Cui, Y. J. (2012). The water retention properties of a natural unsaturated loess from northern France. *Géotechnique*, *62*, 95–106. https://doi.org/10.1680/geot.9.P.084

Omondi, M. O., Xia, X., Nahayo, A., Liu, X., Korai, P. K., & Pan, G. (2016). Quantification of biochar effects on soil hydrological properties using meta-analysis of literature data. *Geoderma*, *274*, 28–34. https://doi.org/10.1016/j.geoderma.2016.03.029

Or, D., & Wraith, J. M. (2002). Soil water content and water potential relationships. In A. W. Warrick (Ed.), *Soil physics companion* (pp. 49–84). CRC Press.

Osán, J., de Hoog, J., Van Espen, P., Szaloki, I., Ro, C.-U., & Van Grieken, R. (2001). Evaluation of energy-dispersive X-ray spectra of low-Z elements from electron-probe microanalysis of individual particles. *X-ray Spectrometry*, *30*, 419–426. https://doi.org/10.1002/xrs.523

Pagliai, M., Vignozzi, N., & Pellegrini, S. (2004). Soil structure and the effect of management practices. *Soil & Tillage Research*, *79*, 131–143. https://doi.org/10.1016/j.still.2004.07.002

Payen, F. T., Sykes, A., Aitkenhead, M., Alexander, P., Moran, D., & MacLeod, M. (2021). Soil organic carbon sequestration rates in vineyard agroecosystems under different soil management practices: A meta-analysis. *Journal of Cleaner Production*, *290*, 125736. https://doi.org/10.1016/j.jclepro.2020.125736

Pertassek, T., Peters, A., & Durner, W. (2015). *HYPROP-FIT software user's manual, V.3.0*. UMS GmbH.

Peters, A., & Durner, W. (2008). Simplified evaporation method for determining soil hydraulic properties. *Journal of Hydrology*, *356*, 147–162. https://doi.org/10.1016/j.jhydrol.2008.04.016

Petersen, C. T., Hansen, E., Larsen, L. V., Ahrenfeldt, J., & Hauggaard-Nielsen, H. (2016). Pore-size distribution and compressibility of coarse sandy subsoil with added biochar. *European Journal of Soil Science*, *67*, 726–736. https://doi.org/10.1111/ejss.12383

Poeplau, C., & Dechow, R. (2023). The legacy of one hundred years of climate change for organic carbon stocks in global agricultural topsoils. *Scientific Reports*, *13*, 7483. https://doi.org/10.1038/s41598-023-34753-0

Poeplau, C., & Don, A. (2015). Carbon sequestration in agricultural soils via cultivation of cover crops—A meta-analysis. *Agriculture, Ecosystems & Environment*, *200*, 33–41. https://doi.org/10.1016/j.agee.2014.10.024

Pollet, S., Chabert, A., Burgeon, V., Cornélis, J.-T., Fouché, J., Gers, C., Hardy, B., & Pey, B. (2022). Limited effects of century-old biochar on taxonomic and functional diversities of collembolan communities across land-uses. *Soil Biology and Biochemistry*, *164*, 108484. https://doi.org/10.1016/j.soilbio.2021.108484

Prakongkep, N., Gilkes, R. J., Wisawapipat, W., Leksungnoen, P., Kerdchana, C., Inboonchuay, T., Delbos, E., Strachan, L.-J., Ariyasakul, P., Ketdan, C., & Hammecker, C. (2020). Effects of biochar on properties of tropical sandy soils under organic agriculture. *Journal of Agricultural Science*, *13*, 1–17. https://doi.org/10.5539/jas.v13n1p1

Prietzel, J., Zimmermann, L., Schubert, A., & Christophel, D. (2016). Organic matter losses in German Alps forest soils since the 1970s most likely caused by warming. *Nature Geoscience*, *9*, 543–548. https://doi.org/10.1038/ngeo2732

Purakayastha, T., Chauhan, S. K., Sasmal, S., & Pathak, S. (2015). Biochar carbon sequestration in soil—A myth or reality? *International Journal of Bio-resource and Stress Management*, *6*, 623–630. https://doi.org/10.5958/0976-4038.2015.00097.4

Razzaghi, F., Obour, P. B., & Arthur, E. (2020). Does biochar improve soil water retention? A systematic review and meta-analysis. *Geoderma*, *361*, 114055. https://doi.org/10.1016/j.geoderma.2019.114055

Reynolds, W. D., & Elrick, D. E. (1990). Ponded infiltration from a single ring: I. Analysis of steady flow. *Soil Science Society of America Journal*, *54*, 1233–1241. https://doi.org/10.2136/sssaj1990.03615995005400050006x

Richards, L. A., & Fireman, M. (1943). Pressure plate apparatus for measuring moisture sorption and transmission by soils. *Soil Science*, *56*, 395–404. https://doi.org/10.1097/00010694-194312000-00001

Schäffer, B., Schulin, R., & Boivin, P. (2013). Shrinkage properties of repacked soil at different states of uniaxial compression. *Soil Science Society of America Journal*, *77*, 1930–1943. https://doi.org/10.2136/sssaj2013.01.0035

Schindler, U., von Unold, G., Durner, W., & Müller, L. (2010). Evaporation method for measuring unsaturated hydraulic properties of soils: Extending the range. *Soil Science Society of American Journal*, *74*, 1071–1083. https://doi.org/10.2136/sssaj2008.0358

Shaaban, A., Se, S.-M., Mitan, N. M. M., & Dimin, M. F. (2013). Characterization of biochar derived from rubber wood sawdust through slow pyrolysis on surface porosities and functional groups. *Procedia Engineering*, *68*, 365–371. https://doi.org/10.1016/j.proeng.2013.12.193

Singh, H., Northup, B. K., Rice, C. W., & Prasad, P. V. V. (2022). Biochar applications influence soil physical and chemical properties, microbial diversity, and crop productivity: A meta-analysis. *Biochar*, *4*, 8. https://doi.org/10.1007/s42773-022-00138-1

Sun, Z., Moldrup, P., Elsgaard, L., Arthur, E., Bruun, E. W., Hauggaard-Nielsen, H., & de Jonge, L. W. (2013). Direct and indirect short-term effects of biochar on physical characteristics of an arable sandy loam. *Soil Science*, *178*, 465–473. https://doi.org/10.1097/SS.0000000000000010

Wang, M., Yu, X., Weng, X., Zeng, X., Li, M., & Sui, W. (2023). Meta-analysis of the effects of biochar application on the diversity of soil

bacteria and fungi. *Microorganisms*, *11*, 641. https://doi.org/10.3390/microorganisms11030641

Whitehead, D., McNeill, S. J. E., & Mudge, P. L. (2021). Regional and national changes in soil carbon stocks with land-use change from 1990 to 2016 for New Zealand. *Regional Environmental Change*, *21*, 121. https://doi.org/10.1007/s10113-021-01837-4

Woolf, D., Amonette, J. E., Street-Perrott, F. A., Lehmann, J., & Joseph, S. (2010). Sustainable biochar to mitigate global climate change. *Nature Communications*, *1*, 56. https://doi.org/10.1038/ncomms1053

Yi, S., Chang, Y. C., & Imhoff, P. T. (2020). Predicting water retention of biochar enriched soil from independent measurements of biochar and soil properties. *Advances in Water Resources*, *142*, 103638. https://doi.org/10.1016/j.advwatres.2020.103638

Zanutel, M., Garré, S., & Bielders, C. (2021). Long-term effect of biochar on physical properties of agricultural soils with different textures at pre-industrial charcoal kiln sites in Wallonia (Belgium). *European Journal of Soil Science*, *73*, e13157. https://doi.org/10.1111/ejss.13157

Zhang, L., Jing, Y., Xiang, Y., Zhang, R., & Lu, H. (2018). Responses of soil microbial community structure changes and activities to biochar addition: A meta-analysis. *Science of The Total Environment*, *643*, 926–935. https://doi.org/10.1016/j.scitotenv.2018.06.231

Zhang, Q., Du, Z., Lou, Y., & He, X. (2015). A one-year short-term biochar application improved carbon accumulation in large macroaggregate fractions. *Catena*, *127*, 26–31. https://doi.org/10.1016/j.catena.2014.12.009

Zhang, Q., Song, Y., Wu, Z., Yan, X., Gunina, A., Kuzyakow, Y., & Xiong, Z. (2020). Effects of six-year biochar amendment on soil aggregation, crop growth, and nitrogen and phosphorus use efficiencies in a rice-wheat rotation. *Journal of Cleaner Production*, *242*, 118435. https://doi.org/10.1016/j.jclepro.2019.118435

How to cite this article: Zanutel, M., Garré, S., Sanglier, P., & Bielders, C. (2023). Biochar modifies soil physical properties mostly through changes in soil structure rather than through its internal porosity. *Vadose Zone Journal*, e20301. https://doi.org/10.1002/vzj2.20301